ACS APPLIED MATERIALS & INTERFACES

Research Article

Cite This: ACS Appl. Mater. Interfaces 2019, 11, 22171−22180

www.acsami.org

Small, Traceable, Endosome-Disrupting, and Bioresponsive Click Nanogels Fabricated via Microfluidics for CD44-Targeted Cytoplasmic Delivery of Therapeutic Proteins

Ke Huang,[†] Yahui He,[†] Zhehong Zhu,[†] Jiakun Guo,[†] Guanglin Wang,[‡] Chao Deng,*[,†] and Zhiyuan Zhong*[,†]

[†]Biomedical Polymers Laboratory, and Jiangsu Key Laboratory of Advanced Functional Polymer Design and Application, College of Chemistry, Chemical Engineering and Materials Science, and State Key Laboratory of Radiation Medicine and Protection, Soochow University, Suzhou 215123, China

[‡]School of Radiation Medicine and Protection and School for Radiological and Interdisciplinary Sciences, Medical College of Soochow University, Suzhou 215123, China

Supporting Information

ABSTRACT: Nanogels (NG) are among the most ideal cytoplasmic protein delivery vehicles; however, their performance is suboptimal, partly owing to relatively big size, poor cell uptake, and endosomal entrapment. Here, we developed small, traceable, endosome-disrupting, and bioresponsive hyaluronic acid NG (HA-NG) for CD44-targeted intracellular delivery of therapeutic proteins. With microfluidics and catalyst-free photo-click cross-linking, HA-NG with hydrodynamic diameters of ca. 80 and 150 nm, strong green fluorescence and efficient loading of various proteins including saporin (Sap), cytochrome C, herceptin, immunoglobulin G (IgG), and bovine serum albumin could be fabricated. Interestingly, 80 nm-sized HA-NG revealed clearly better cellular uptake than its 150 nm counterparts in both CD44-negative U87 cancer cells and CD44-positive 4T1 and MDA-MB-231 cells. Moreover, small NG exhibited accelerated endosomal escape, which was further boosted by introducing GALA, a pH-sensitive fusogenic peptide. Accordingly, Sap-loaded small and GALA-functionalized HA-NG showed the highest cytotoxicity in CD44-positive MDA-MB-231, 4T1, A549, and SMMC-7721 cancer cells. The biodistribution studies demonstrated that 80 nm-sized HA-NG displayed significantly greater tumor uptake as well as penetration in MDA-MB-231 human breast tumor xenografts than its 150 nm counterparts, whereas the introduction of GALA had no detrimental effect on tumor accumulation. Small, endosome-disrupting, and bioresponsive HA-NG with easy and controlled fabrication hold a great potential for targeted protein therapy.

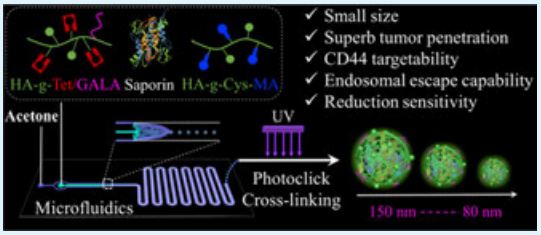

KEYWORDS: *nanogels, microfluidics, click reaction, endosomal escape, protein delivery, cancer therapy*

1. INTRODUCTION

Proteins with intracellular targets, such as granzyme B and saporin (Sap), can potently inhibit the proliferation of various cancer cells.[1−3] However, their clinical translation is impeded by inefficient cellular uptake and fast enzymatic degradation.[4−6] Nanogels (NG) with excellent biocompatibility, protein compatibility, and protein loading have been extensively exploited for protein delivery in recent years.[7−11] Specifically, NG can greatly increase the in vivo stability, circulation time, and tumor accumulation of proteins.[12−14] Various methods, including inverse nanoprecipitation,[15,16] in situ self-assembly,[17,18] and inverse mini-emulsion,[19,20] have been employed to prepare NG. However, these strategies generally suffer from modest control on size and size distribution of NG, and the formed NG often exhibit an average size of bigger than 100 nm, which might compromise their cellular uptake and tumor penetration. Microfluidics technology providing superior control of particle sizes has been exploited to prepare defined nanoparticles with controllable size and narrow size distribution.[21−24] The biophysical properties of nanoparticles can be tailored by flow rate, precursor composition, and concentration.

To boost the cellular uptake and selectivity of NG in cancer cells, different target ligands and polymers have been exploited to develop advanced NG for protein delivery.[9,10] For example, targeting peptides like LHRH, GE11, and VNTANST have been decorated on the surface of NG to achieve the targeted delivery of tumor suppressor protein p53, granzyme B, and shikonin, leading to significant apoptosis of MDA-MB-231 breast, SKOV-3 ovarian, and osteosarcoma cancer cells, respectively.[25−27] Hyaluronic acid, which can target CD44 overexpressing cancer cells, has been exploited to construct NG for efficient loading of therapeutic proteins (granzyme B, saporin, deoxyribonuclease I, etc.),[17,28−30] which exhibited

Received: April 3, 2019
Accepted: June 3, 2019
Published: June 3, 2019

DOI: 10.1021/acsami.9b05827
ACS Appl. Mater. Interfaces 2019, 11, 22171−22180

Scheme 1. Schematic Illustration of Small, Traceable, Endosome-Disrupting, and Bioresponsive Click NG Fabricated via Microfluidics for CD44-Targeted Cytoplasmic Delivery of Therapeutic Proteins

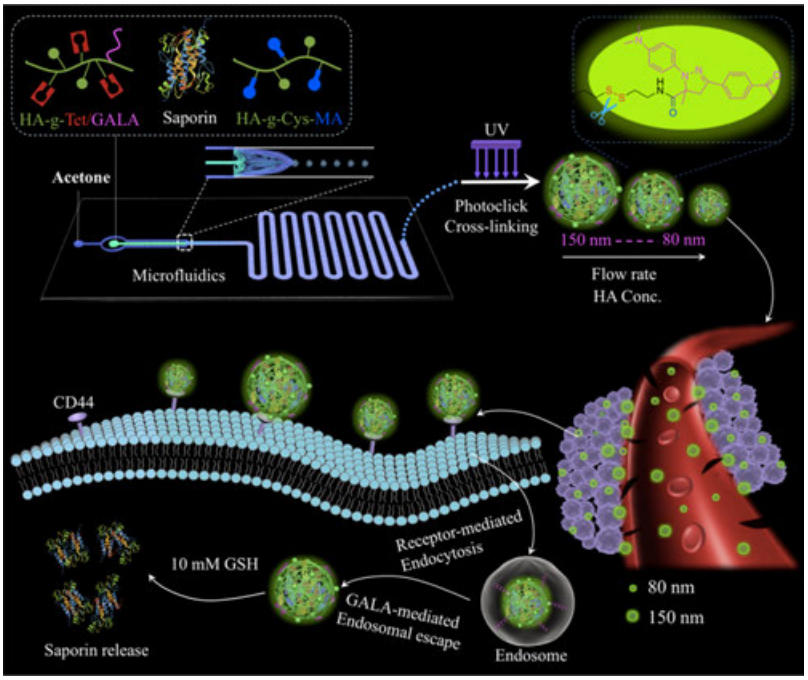

significant growth suppression of MCF-7, A549, and HCT-116 tumor xenografts at low doses. Considering the enzyme-rich and acidic environments of endosomes, endosomal escape is crucial for therapeutic proteins encapsulated in NG to take effect inside cancer cells.[31] Cell penetrating peptide (CPP) and fusion peptides have been used to promote the cytoplasmic delivery of proteins.[32,33] CPP assists the nanocarriers escape from endosomes by directly penetrating the endosomal membrane, whereas the fusion peptide disrupts the endosomal membrane by pH-dependent conformational changes and membrane fusion.

Here, we developed small, traceable, endosome-disrupting, and bioresponsive hyaluronic acid NG (HA-NG) for CD44-targeted intracellular delivery of therapeutic proteins (Scheme 1). NG were fabricated from HA derivatives, that is, HA-*g*-cystamine-methacrylate (HA-*g*-Cys-MA) and HA-*g*-lysine-tetrazole/GALA (HA-*g*-Tet/GALA), by employing the microfluidics technique and catalyst-free photo-click reaction. Microfluidics would afford controlled fluid and mixing, resulting in uniform products, tunable sizes, and high output.[34,35] The catalyst-free click reaction possesses high specificity, high efficiency, and no toxicity, which is important to prevent proteins from denaturation and NG from toxic contamination. The incorporation of cystamine into the HA-*g*-Cys-MA derivative would offer reduction responsivity. HA can target CD44 high-expressing tumor cells, including human breast, lung, and liver tumor cells (MDA-MB-231, A549, and SMMC-7721).[36] GALA, a synthetic anionic peptide and maintains random coil conformation under neutral condition and transits into a α-helix structure under endosomal acidic condition (pH < 6), has shown a high endosome-disrupting potency.[37,38] The incorporation of GALA in NG would boost the endosome escape of NG. Our results showed that HA-NG with a small size of 80 nm exhibit significantly enhanced tumor uptake as well as penetration in MDA-MB-231 human breast tumor xenografts, and Sap-loaded small and GALA-functionalized HA-NG display the highest cytotoxicity in CD44-positive cancer cells.

2. EXPERIMENTAL SECTION

2.1. Synthesis of HA-*g*-Tet/GALA. HA-*g*-Tet/GALA was fabricated through an amidation reaction between GALA-NH_2 and carboxyl groups of HA-*g*-Tet (Scheme S1), which was acquired according to our previous report.[41] Briefly, EDC (21.6 mg, 112.5 μmol) and NHS (25.8 mg, 225 μmol) were added to a solution of HA-*g*-Tet (43.4 mg, 75 μmol of −COOH) in deionized (DI) water (4.4 mL) to activate the carboxyl groups of HA. After proceeding at 25 °C for 15 min, a solution of GALA (10.0 mg, 3 μmol) in 1 mL of dimethyl sulfoxide (DMSO) was added to the above solution, and the pH was adjusted to 8.0−9.0 using a NaOH solution (2.0 M). The reaction mixture was stirred for 24 h at 40 °C and then dialyzed (spectra/pore, MWCO of 3.5 kDa) against a mixed solution of DI water/DMSO (1:1, v/v) and DI water. HA-*g*-Tet/GALA was collected by lyophilization. Yield: 95.4%. The molar amount of GALA was quantified by a microBCA assay. In brief, HA-*g*-Tet/GALA (1 mg/mL, 150 μL) and microBCA fluid (150 μL) were added in a 96-well plate and then incubated at 37 °C for 2 h. The amount of GALA was determined by measuring the absorbance at λ = 570 nm with a microplate reader. Free GALA with concentrations of 2−40 μg/mL was employed to obtain the standard curves. The degree of substitution (DS) defined as the molar amount of GALA per 100 sugar units was 4.0.

2.2. Fabrication of HA-NG via Microfluidics and Photo-Click Cross-Linking. The microfluidic chip fabricated with soda lime glass consists of three parallel inlet channels with a length of 10 mm, a width of 0.2 mm, and a height of 0.4 mm, which are converged to a long rectangular channel (2 mm wide, 0.4 mm high, 20 mm long) (Scheme S2). Nanodroplets were formed at the intersection of three inlets, where the central water phase containing HA-*g*-Tet and HA-*g*-Cys-MA at a Tet/MA molar ratio of 1:1 was converged with the oil phase (acetone) passing through two side channels. The flow rate ratio of the aqueous phase to the oil phase was fixed at 1:5. The obtained dispersion of nanodroplets (12 mL) was collected in the outlet channel and then settled in a disc with a diameter of 15 mm. After 60 s of UV irradiation (320−390 nm, 50 mW/cm^2), the oil was evaporated by a rotary evaporator. Afterward, HA-NG were purified

DOI: 10.1021/acsami.9b05827
ACS Appl. Mater. Interfaces 2019, 11, 22171−22180

by dialyzing (spectra/pore, MWCO of 3500) against DI water. Yield: 83%. GALA was introduced into NG by adding HA-*g*-Tet/GALA into the polymer solution prior to administration in the microfluidic chip. The average number of GALA in 100 sugar units of HA chain in NG was adjusted as 0.5, 1.0, and 1.5 by changing the molar feed ratios of HA-*g*-Tet, HA-*g*-Tet/GALA, and HA-*g*-Cys-MA (Table S1), and the corresponding NG were denoted as NG/GALA-0.5, NG/GALA-1.0, and NG/GALA-1.5, respectively. Protein-loaded NG were similarly fabricated except that the solution of various proteins, like Sap, cytochrome C, herceptin, IgG, or bovine serum albumin (BSA), was mixed with HA derivatives prior to injecting into the middle stream of the microfluidics chip. The size of NG with or without proteins was measured four times per sample with dynamic laser scattering (DLS, Zetasizer Nano-ZS, Malvern Instruments) at 25 °C in water. The morphology of the NG was acquired by a transmission electron microscopy (TEM; Tecnai G220) instrument at an accelerating voltage of 200 kV. The samples were prepared by depositing 10 μL of NG dispersion (200 μg/mL) on the copper grid for 15 min followed by staining with phosphotungstic acid (1 wt %) for 50 s.

2.3. In Vitro Release of Sap from HA-NG. The release of Sap from HA-NG was performed in phosphate buffer (PB, 10 mM pH 7.4), with or without reduced glutathione (GSH) (10 mM), at 37 °C via the dialysis method. First, 0.2 mL of protein-loaded HA-NG dispersion following transfer to a dialysis bag (MWCO: 300 kDa) was submerged in 25 mL of phosphate-buffered saline (PBS) and then placed in an incubator at 37 °C with shaking at 200 rpm. The release medium was purged with nitrogen to avoid the oxidation of GSH. At desired time intervals, 5 mL of the release medium was taken out and refilled with an equal volume of fresh medium. The collected release solutions were dialyzed against DI water to remove GSH, and then the amount of proteins was quantified by microBCA assays. Protein loading content (PLC) and protein loading efficiency (PLE) were calculated according to eqs 1 and 2, respectively.

$$\text{PLC (wt \%)} = \text{(weight of protein/total weight of polymer and protein)} \times 100 \quad (1)$$

$$\text{PLE (\%)} = \text{(weight of loaded protein/weight of protein in feed)} \times 100 \quad (2)$$

2.4. Cellular Uptake and Intracellular Trafficking Behaviors of NG. Cellular uptake and intracellular trafficking behaviors of NG with different sizes were explored in several cancer cells, including 4T1, MDA-MB-231, and U87 cells. Typically, cells (3×10^5 cells/well) were seeded in a 6-well plate with 800 μL culture medium (RPMI 1640 for 4T1 cells and Dulbecco's modified Eagle's medium (DMEM) for MDA-MB-231 and U87 cells) containing 10% (v/v) fetal bovine serum, 1% (v/v) antibiotics penicillin (100 IU/mL) and streptomycin (100 μg/mL) overnight at 37 °C under a CO_2 atmosphere (5%). Cy5-labeled NG (200 μg/mL) in 200 μL DI water were added and incubated with the cells for 4 h. Subsequently, the cells were digested with trypsin, centrifuged at 1000 rpm for 3 min, washed twice with PBS, and dispersed in 500 μL of PBS. Ten thousand cells were collected to generate histograms using flow cytometer (BD FACS Calibur, USA).

For confocal laser scanning microscopy (CLSM) measurement, MDA-MB-231 cells (1×10^5 cells/well) were similarly cultured on microscope slides in a 24-well plate with DMEM for 24 h. 100 μL of HA-NG (500 μg/mL) with intrinsic fluorescence in DI water was added to each well and incubated for 4 h; then the cells were fixed with 4% paraformaldehyde solution for 15 min. Cytoskeleton was stained by phalloidin−tetramethyl-rhodamine B isothiocyanate (red) for 40 min. The fluorescence images were obtained using a confocal microscope (Leica TCS SP2). For endosomal escape studies, MDA-MB-231 cells were treated with HA-NG in the same pattern as above. Then, endosomes were stained by Lysotracker-red (150 nM) for 40 min, and the cells were fixed with 4% paraformaldehyde solution for 15 min. The fluorescence images were taken by a confocal microscope (Leica TCS SP2).

2.5. In Vitro Cytotoxicity of Sap-NG. CD44-positive 4T1, MDA-MB-231, A549, and SMMC-7721 cancer cells were chosen to explore the in vitro cytotoxicity of Sap-loaded NG (Sap-NG) using 3-(4,5-dimethylthiazol-2-yl)-2,5-diphenyl tetrazoliumbromide (MTT) assay. Briefly, 4T1 (1×10^3 cells/well), MDA-MB-231 (2.5×10^3 cells/well), A549 (2×10^3 cells/well), or SMMC-7721 cells (2×10^3 cells/well) were plated in 96-well plates and cultured in media supplemented with 10% (v/v) fetal bovine serum and antibiotics penicillin (100 IU/mL) and streptomycin (100 μg/mL) for 24 h in 5% CO_2 atmosphere at 37 °C. Sap-NG with different concentrations in DI water (20 μL) were added. After 4 h, the culture medium was re-freshed, and the cells were incubated for another 92 h. Subsequently, MTT solution in PBS (10 μL, 5 mg/mL) was added to each well and incubated for 4 h in the dark. Following the careful removal of the supernatant, 150 μL of DMSO was added to dissolve the MTT-formazan crystals, which was measured by a microplate reader (Bio-Tek, ELX808IU) with the absorbance at 490 nm. The cell viability was defined as the percentage of the absorbance of the viable cells treated with Sap-NG to that of the cells treated with PBS. The IC_{50} was calculated by curve fitting of the cell viability versus protein concentrations ($n = 4$). The biocompatibility of blank NG was similarly investigated using the MTT assay.

2.6. In Vivo Pharmacokinetics and Biodistribution. The mice were handled under protocols approved by Soochow University Laboratory Animal Center and the Animal Care and Use Committee of Soochow University. To explore the in vivo pharmacokinetics and biodistribution, free Sap was labeled with radioactive ^{125}I. Briefly, 800 μL of Sap (10 μg/mL), 200 μCi of $Na^{125}I$, and 10 μL of 10 mg/mL chloramine-T were thoroughly mixed, and the reaction proceeded at room temperature for 20 min. Then, 10 μL of $Na_2S_2O_5$ (10 mg/mL) was added. After stirring for 10 min, unreacted ^{125}I was removed by extensive dialysis against DI water (MWCO = 3.5 kDa). The reaction efficiency determined by the gamma counter was 50%. Sap-NG were similarly labeled with $Na^{125}I$ in DI water, and the reaction efficiency was 15%. For in vivo pharmacokinetic study, female BALB/c mice ($n = 3$) were intravenously injected with ^{125}I-labeled free Sap (^{125}I-Sap) and Sap-NG (^{125}I-Sap-NG). At 0.05, 0.25, 0.5, 1, 2, 4, 6, 8, 10, and 24 h, around 30 μL of blood was collected from the mice. Sap in blood samples was quantitated by the gamma counter. The elimination half-life ($t_{1/2\beta}$) of Sap was determined by fitting the experimental data using the software Origin 9 exponential decay 2 model: $y = A_1 \exp(-x/t_1) + A_2 \exp(-x/t_2) + y_0$, and taking $t_{1/2\beta} = 0.693 \times t_2$.

4T1 tumor established by injecting 5×10^5 4T1 cells suspended in PBS (50 μL) into the subcutaneous of nude mice ($n = 3$) was employed to evaluate the in vivo biodistribution. The tumor-bearing mice were intravenously injected with ^{125}I-Sap-NG or ^{125}I-Sap. At 6 h post iv injection, the tumor and major organs were collected, and the amount of Sap was determined by the gamma counter.

In vivo imaging was further employed to investigate the tumor targetability of NG with different sizes (80 and 150 nm). Cy5-labeled NG were injected into nude mice (female, 6 weeks old) bearing 4T1 tumor via the tail vein at a concentration of 200 μg/mL. The tumor fluorescence images were obtained by a near-infrared fluorescence imaging system (IVIS Lumina II, Caliper, MA) at 2, 6, 12, and 24 h post-injection.

2.7. Ex Vivo Tumor Penetration. MDA-MB-231 human breast tumors were established by subcutaneously inoculating MDA-MB-231 cells (1×10^7 cells per mouse) to nude mice (female, 5 weeks old) at the left flank. When the tumors grew up to 150−200 mm^3, mice were sacrificed. The harvested tumors were ex vivo cultured with NG-80 or NG-150 (1 mg/mL) in DMEM media supplemented with 10% (v/v) fetal bovine serum and antibiotics penicillin (100 IU/mL) and streptomycin (100 μg/mL) in a 24-well plate for 48 h. The tumors were collected and fixed by 4% formalin for 24 h. Tumor sections (20 μm thickness) were collected and mounted on glass slides. The fluorescence and brightfield images were taken by a confocal microscope (Leica TCS SP2).

DOI: 10.1021/acsami.9b05827
ACS Appl. Mater. Interfaces 2019, 11, 22171−22180

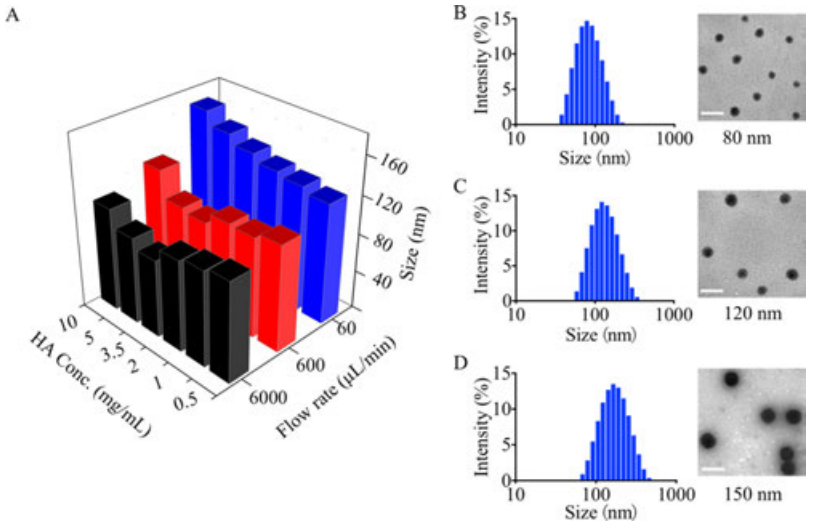

Figure 1. Size changes of HA-NG with varying polymer concentrations and flow rates. (A) Mean NG size map controlled by adjusting HA concentrations and flow rates (n = 4). DLS measurement and TEM images of NG with average diameters of 80 (B), 120 (C), and 150 nm (D). Scales: 200 nm.

3. RESULTS AND DISCUSSION

3.1. Fabrication of HA-NG via Microfluidics and Photo-Click Cross-Linking. Traceable bioresponsive NG were fabricated from HA-*g*-Cys-MA and HA-*g*-Tet using the microfluidics technique and catalyst-free photo-click reaction (Scheme S3). The convergent channel in the microfluidics chip created tunable symmetric microvortices and a different focusing pattern, generating nanodroplets with defined sizes and size distribution. Following covalent cross-linking via a catalyst-free "tetrazole−alkene" click reaction, stable NG were formed. Figure S1 shows that the absorbance at 275 nm belonged to the tetrazole groups of HA-*g*-Tet completely disappeared in NG after UV irradiation for 60 s, signifying the fast reaction and thorough cross-linking of NG. The formed NG exhibited tunable sizes (80−160 nm), depending on flow rates and polymer concentrations (Figure 1A). The size of NG was observed to decrease with increasing total flow rates from 60 to 6000 μL/min and decreasing polymer concentrations from 10.0 to 3.5 mg/mL. Faster flow rates and higher solution viscosity (polymer concentration) corresponding to bigger Reynolds number (*Re*) for microfluidics have been reported to generate smaller nanoparticles.[39] As characterized by DLS and TEM, HA-NG displayed a spherical morphology and controllable defined sizes (Figure 1B−D). In the following, NG with diameters 80 nm (Table 1, entry 1) and 150 nm (Table 1, entry 5) are referred to as NG-80 and NG-150, respectively. Comparing with the traditional nanoprecipitation method,[29] the microfluidics technique generated NG with smaller and more controlled sizes (Figure S2). Besides, much less (1/8.3) acetone and UV irradiation time (1 vs 3 min) are required for the microfluidics technique. We further investigated the influence of molecular weight and DS of HA derivatives on the NG size. The results showed that although the DS of HA derivatives had little influence on the NG size, HA with a higher molecular weight (35 kg/mol) produced NG with bigger sizes, possibly owing to augmented solution viscosity and decreased *Re* (Table 1). To exploit the effect of cross-linking density, HA-Lys-Tet with a DS of 10 (Table 1, entry 2) was employed to form NG-80 with a higher cross-linking density, which is denoted as NG-80/HX in the following. In addition, the decoration of GALA in NG was observed to have little influence on its size.

Table 1. Characteristics of HA-NG

entry[a]	M_w of HA (kg/mol)	DS of Tet	DS of MA	size (nm)[b]	PDI[b]	zeta (mV)[c]
1	20	5	5	83.6	0.13	−15.7
2	20	10	5	82.4	0.14	−15.9
3	36	10	5	98.1	0.12	−16.4
4	36	10	10	96.7	0.11	−16.2
5[c]	20	5	5	153.1	0.10	−17.9

[a]Entries 1−4: polymer concentration: 3.5 mg/mL, flow rates: 6000 μL/min; entry 5: polymer concentration: 5 mg/mL, flow rates: 60 μL/min. [b]Determined by DLS at 25 °C in water. [c]Determined by Zetasizer Nano-ZS equipped with an electrophoresis cell at 25 °C in water.

NG displayed a negatively charged surface with zeta potentials of around −16 mV and intrinsic fluorescence resulting from formed pyrazoline groups in the NG (Figure 2A). Similar intrinsic fluorescence was also observed in the polymer, NG, and microgels formed via the "tetrazole−alkene" photo-click reaction.[40−42] The fluorescence intensity increased with increasing DS of HA derivatives, and the strong fluorescence facilitates the tracking of cellular uptake and tumor penetration behaviors of HA-NG. Besides, HA-NG displayed high stability and showed little size change following extensive dilution and one-week storage at 4 °C (Figure 2B−C). In the presence of GSH, NG showed obvious swelling and aggregation in 24 h owing to the cleavage of disulfide bonds, signifying the reduction sensitivity of NG.

3.2. Protein Loading and Release. Proteins, including Sap, cytochrome C, herceptin, BSA, and IgG, could be easily loaded into HA-NG by mixing proteins with the polymer solution before injecting into the inlet of the microfluidic chip. The results showed that all proteins could be efficiently encapsulated into NG-80, and the PLE ranged from 73.4 to 97.1% at a theoretical PLC of 5 wt % (Table 2). Protein loading in NG was observed to have little influence on their size, size distribution, and surface charge. NG-150 exhibited equivalent loading capacity for the above five proteins. Using

DOI: 10.1021/acsami.9b05827
ACS Appl. Mater. Interfaces 2019, 11, 22171−22180

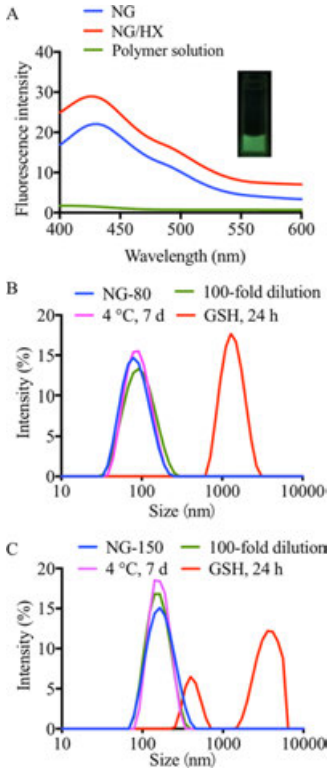

Figure 2. (A) Fluorescence emission spectra of NG-80, NG-80/HX, and polymer solution at an excitation wavelength of 365 nm. The inset shows the fluorescent image of HA-NG. Colloidal stability of NG-80 (B) and NG-150 (C) at 1.0 mg/mL in water for 7 days, against 100-fold dilution, and 10 mM GSH.

Table 2. Characteristic of Protein-Loaded NG-80

	PLC (wt %)					
protein	theory	determined	PLE (%)	size (nm)[a]	PDI[a]	zeta (mV)[b]
cytochrome C	5	4.8	96.3	78.4	0.11	−15.0
	10	8.9	87.9	81.8	0.12	−13.9
Sap	5	3.8	73.4	80.7	0.13	−15.1
	10	5.7	54.4	82.3	0.16	−14.5
BSA	5	4.0	76.9	88.4	0.15	−16.3
	10	7.5	73.3	91.5	0.14	−17.4
herceptin	5	4.8	96.0	82.8	0.10	−15.2
	10	8.6	84.6	87.2	0.13	−14.3
IgG	5	4.8	97.1	79.3	0.12	−14.9
	10	9.5	94.6	84.5	0.14	−13.8

[a]Determined by DLS at 25 °C in water. [b]Determined by a Zetasizer Nano-ZS equipped with an electrophoresis cell at 25 °C in water.

the microfluidics technique, small physically cross-linked NG were elegantly developed from HA-*g*-octenyl succinic acid and alginate/Ca^{2+}, respectively, though they showed poor stability and drug loading because of weak cross-linking.[43,44] Although Sap-loaded NG exhibited high stability with less than 20% protein release in 24 h under physiological conditions, fast protein release was observed in the presence of GSH (Figure 3A). The protein release behaviors were found to be related with the cross-linking density of NG, and NG-80/HX exhibited a slightly lower release of Sap in comparison with NG-80 within 24 h. However, the NG with different sizes of 80 and 150 nm displayed similar release behaviors in the absence/presence of GSH. Of note, the released Sap revealed an

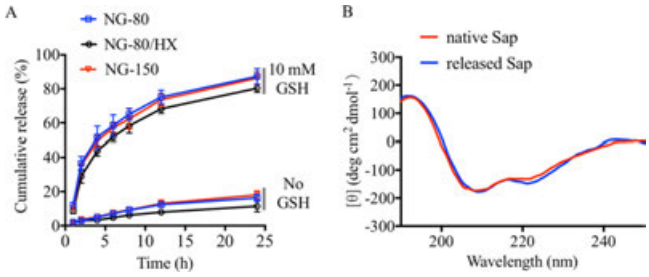

Figure 3. (A) In vitro release of Sap from NG-80, NG-80/HX, and NG-150 in PB with or without 10 mM GSH. (B) Circular dichroism spectra of native Sap and released Sap.

equivalent secondary structure to the native one (Figure 3B), indicating that the loading process has little influence on the structure of encapsulated proteins.

3.3. Cellular Uptake, in Vitro Cytotoxicity, and Endosomal Escape. The cellular uptake behaviors of NG with different sizes were investigated in both CD44-positive (4T1 and MDA-MB-231) and CD44-negative (U87) cancer cells. Flow cytometry measurement revealed that NG-80 had over twofold stronger fluorescence intensity than NG-150 in all tested cells (Figure 4A−C), suggesting that NG with a smaller size had higher cellular uptake whether in CD44-positive or CD44-negative cells. Other nanovehicles, including silica, Au, and polymeric nanoparticles, with a smaller size have also been observed to have higher cellular uptake in different cancer cells.[45−48] Taking advantages of the intrinsic fluorescence of NG, their cellular uptake was further observed using CLSM. The results showed that the cells treated with NG-80 exhibited much stronger NG fluorescence than those incubated with NG-150 in the cytoplasm of MDA-MB-231 cells (Figure 4D), supporting that small size benefits the cellular uptake of NG.

In the following, the cytotoxicity of Sap-NG was evaluated using the MTT assay in CD44-positive 4T1, MDA-MB-231, A549, and SMMC-7721 cancer cells. Sap-NG could efficiently inhibit cell proliferation with an IC_{50} ranging from 13.1 to 25.7 nM in the four tested cancer cells (Figure 5A−D). In line with the higher cellular uptake of NG with smaller sizes, NG-80 generated higher cytotoxicity and lower IC_{50} in comparison with NG-150 in all tested cancer cells (Table 3). By introducing a fusogenic peptide GALA, Sap-NG/GALA exhibited a further enhanced anticancer effect, and NG-80/GALA-1.0 displayed smaller IC_{50} values that were around half of NG-80 without GALA in the tested cancer cells. The elevated anticancer effect of Sap-NG/GALA mainly results from the secondary structure change of GALA from random coil to α-helix, which facilitates the fast endosome escape of protein-loaded NG. In a similar strategy, GALA has been introduced into nanomedicines based on liposomes, polymersomes, and nanoparticles that exhibited enhanced endosome escape.[49−51] Interestingly, NG/GALA-1.0 displayed the lowest IC_{50} in the four tested cancer cells and was thus employed for the following in vitro and in vivo experiments. As shown in Figure S3, cells following the incubation with blank NG (50−800 μg/mL) for 48 h exhibited over 95% cell viability in both 4T1 and MDA-MB-231 cells, illustrating that NG is practically non-cytotoxic.

The endosomal escape of NG/GALA-1.0 was visualized using CLSM. Figure 5E shows that NG/GALA-1.0 following 4 h incubation with MDA-MB-231 cells displayed nearly complete departure from endosomes, as evidenced by the

DOI: 10.1021/acsami.9b05827
ACS Appl. Mater. Interfaces 2019, 11, 22171−22180

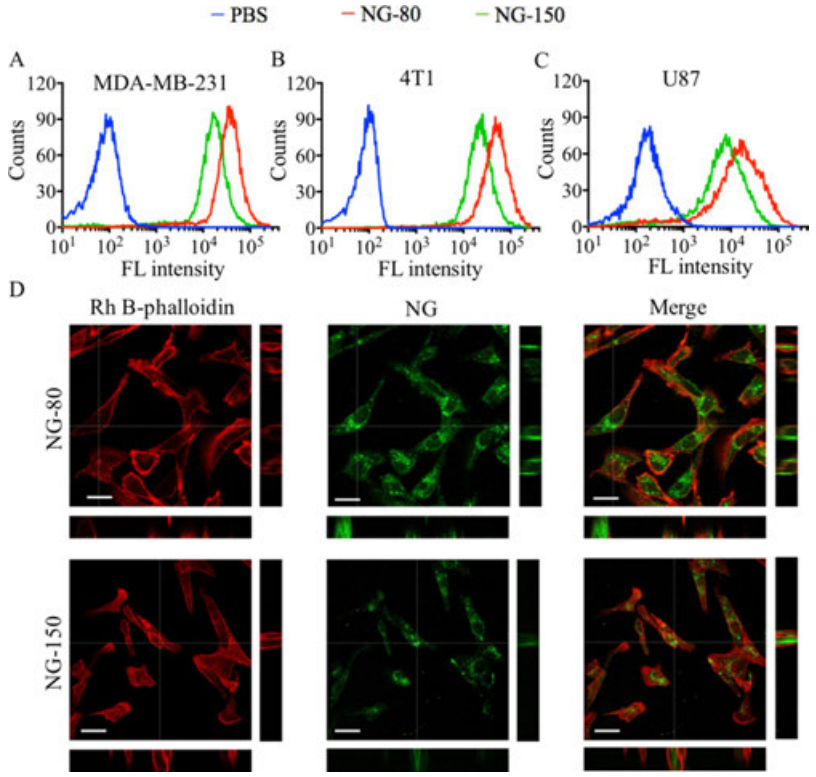

Figure 4. Flow cytometry profile of (A) CD44-positive MDA-MB-231 cells, (B) CD44-positive 4T1 cells, and (C) CD44-negative U87 cells following the treatment with NG for 4 h. (D) CLSM image of MDA-MB-231 cells following the treatment with NG for 4 h. Cytoskeleton was stained by phalloidin−tetramethyl-rhodamine B isothiocyanate (red). Scale bars: 20 μm.

separation of NG (green) from endosomes (red). Under otherwise same conditions, cells treated with NG-80 and NG-150 without GALA displayed a number of yellow points, indicating that most NG colocalize with endo/lysosomes. Meanwhile, NG-80 displayed more dispersed NG fluorescence in the cytoplasm of MDA-MB-231 cells in comparison with NG-150, suggesting that a smaller size benefits the endosomal escape of NG. Considering that Sap takes effect only on ribosome, the endosomal escape is critical for the efficient delivery of Sap by NG.

3.4. In Vivo Pharmacokinetics and Biodistribution. For in vivo pharmacokinetic studies, ^{125}I-Sap-NG and free ^{125}I-Sap were iv injected in mice, respectively. The blood was withdrawn at a predetermined time, and the amount of Sap was quantified by measuring the ^{125}I using the gamma counter. As shown in Figure 6A, all NG followed a typical two-phase pharmacokinetics, that is, a fast distribution phase and a long elimination phase. Both ^{125}I-sap-NG-80 and ^{125}I-sap-NG-150 exhibited a short distribution half-life ($t_{1/2\alpha}$) of 0.12 h, indicating quick distribution of NG in different tissues and organs, like liver and spleen, following iv injection. In comparison with ^{125}I-Sap-NG-80 ($t_{1/2\beta}$ = 3.80 h), ^{125}I-Sap-NG-150 with a bigger size displayed a prolonged elimination half-life ($t_{1/2\beta}$ = 4.65 h). Nanovehicles, like nanosuspension, with a bigger size of 200 nm have been previously observed to have a longer circulation time than their small (70 nm) counterparts ($t_{1/2\beta}$: 40 vs 24 min).[52] The opposite has, however, been reported for poly(ethylene glycol)-coated silica and gold nanoparticles, in which nanoparticles of over 100 nm had a noticeably shorter circulation time than smaller ones (60 nm).[53,54] The different effects of particle size on circulation time might be because of the difference in types and surface characteristics of nanoparticles.[55,56] The incorporation of GALA in NG was observed to have little effect on its circulation time, and both NG-80 and NG-80/GALA had an elimination half-life of around 3.80 h. In sharp contrast, free Sap was rapidly cleared from the systemic circulation and presented a short elimination half-life of 0.69 h.

Biodistribution is one of the key factors that affect the overall therapeutic performance of nanomedicines. Following iv injection in mice bearing 4T1 tumors for 6 h, ^{125}I-Sap-NG with different sizes exhibited much higher protein accumulation at tumor sites than free ^{125}I-Sap (1.94% ID/g), signifying their tumor targetability (Figure 6B). Moreover, ^{125}I-Sap-NG-80 displayed significantly higher accumulation in tumor than ^{125}I-Sap-NG-150 (8.5% ID/g vs 5.9% ID/g, $p < 0.05$), suggesting that NG with smaller sizes have better tumor penetration and retention. ^{125}I-Sap-NG-80/GALA showed an equivalent tumor accumulation to ^{125}I-Sap-NG-80, indicating that GALA functionalization has little effect on tumor accumulation of NG.

The tumor targetability of NG was further investigated by in vivo imaging. The results showed that NG following iv injection could efficiently accumulate at tumor sites in 4T1 tumor-bearing mice during the whole experimental period (2−24 h), in which NG-80 displayed much higher augmentation than NG-150, as characterized by stronger fluorescence intensity from Cy5-labeled NG (Figure S4). Thus, the Sap-loaded NG possesses superb tumor targetability and extended circulation time, and although exhibiting a shorter elimination half-life, smaller NG display higher tumor accumulation.

3.5. Ex Vivo Tumor Penetration. The tumor penetration of nanomedicines is believed to be related with their sizes and plays a critical role in achieving the therapeutic effect.[57,58] To

DOI: 10.1021/acsami.9b05827
ACS Appl. Mater. Interfaces 2019, 11, 22171−22180

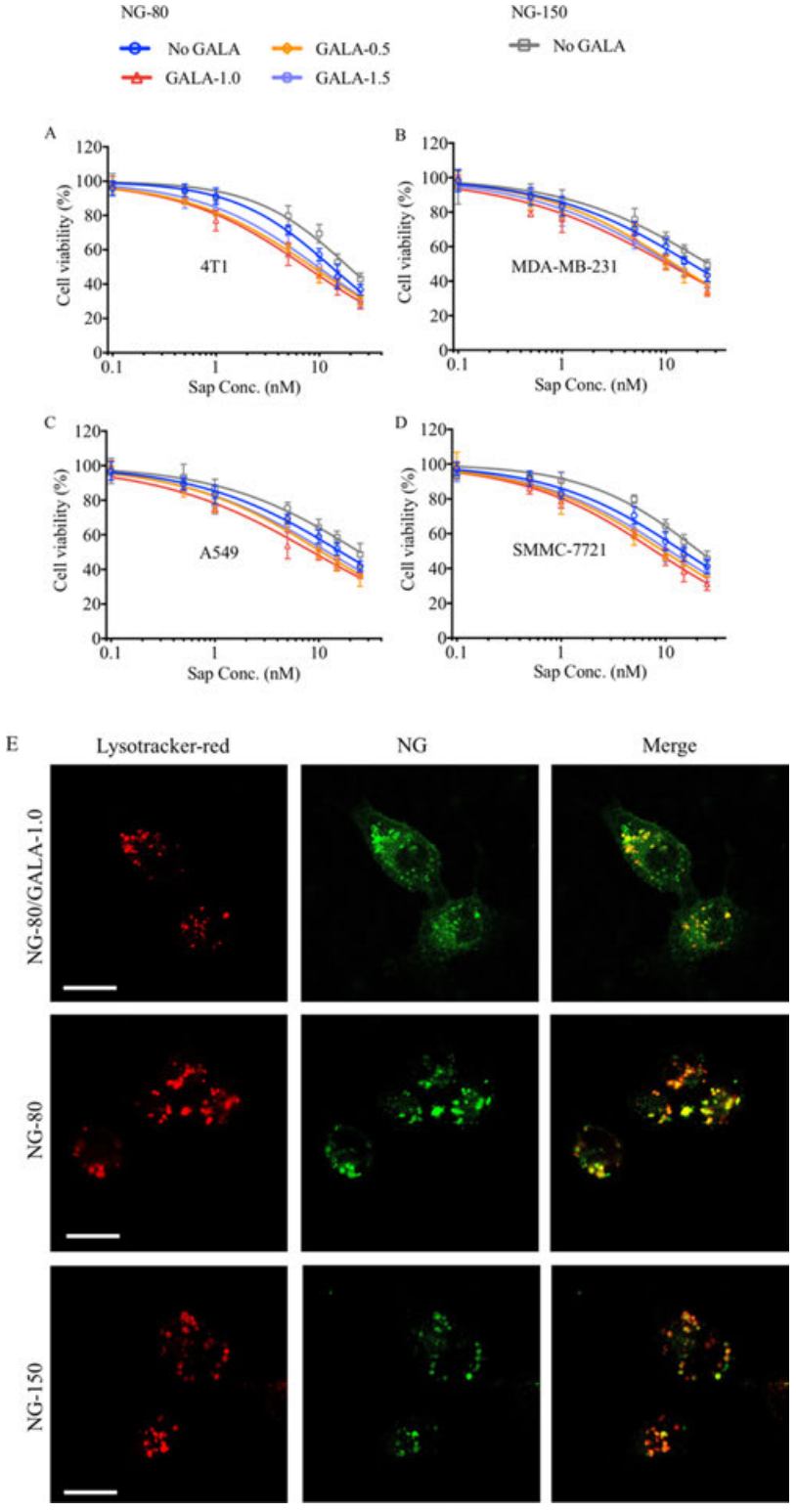

Figure 5. Cell viability of (A) 4T1, (B) MDA-MB-231, (C) A549, and (D) SMMC-7721 cells treated with different Sap-NG groups. Cells were incubated with Sap-NG for 4 h and further cultured in a fresh culture medium for another 92 h. (E) Endosome escape of fluorescent NG-80/GALA-1.0 (green, 200 μg/mL) in 4T1 cells following 4 h incubation. Endosomes were stained by LysoTracker Red (red). Scale bars: 20 μm.

explore the tumor penetration of NG, MDA-MB-231 tumors were established and harvested upon reaching 150−200 mm^3 and then incubated with NG with different sizes. As shown in Figure 6C, the tumor penetration of NG was closely associated with their sizes, in which NG-80 demonstrated much deeper penetration from the periphery of the tumors than NG-150 following 48 h incubation. The quantitative analysis revealed that NG-150 mostly accumulated at the sites that were 150−200 μm away from the tumor periphery, whereas NG-80 group showed a large amount of NG fluorescence at 300−500 μm away from the tumor periphery (Figure 6D). Therefore, the size of NG has a critical effect on their tumor penetration and

DOI: 10.1021/acsami.9b05827
ACS Appl. Mater. Interfaces 2019, 11, 22171−22180

Table 3. IC_{50} Values of Sap-NG in Different Cancer Cells

NG	IC_{50} (nM)			
	4T1 cells	MDA-MB-231 cells	A549 cells	SMMC-7721 cells
NG-80	13.1	17.6	16.4	14.5
NG-80/GALA-0.5	8.6	12.0	10.7	9.5
NG-80/GALA-1.0	7.4	10.3	8.7	7.9
NG-80/GALA-1.5	9.7	11.4	12.2	11.0
NG-150	19.2	25.7	24.8	21.0

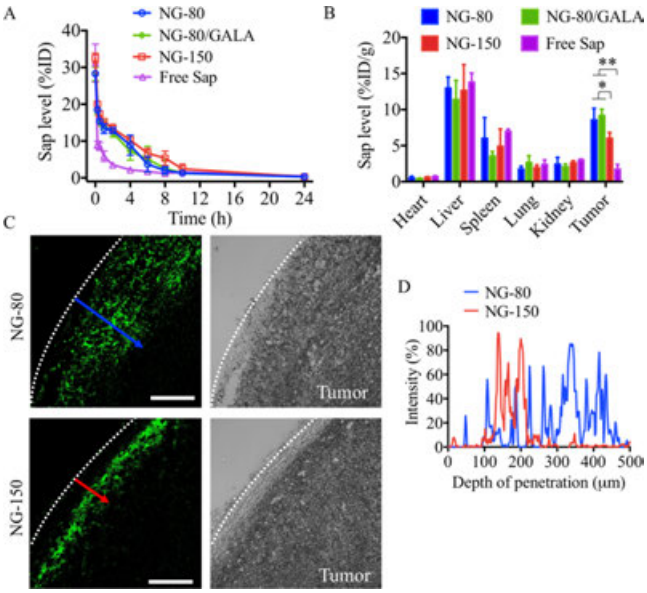

Figure 6. (A) In vivo pharmacokinetics of ^{125}I-Sap-NG and free ^{125}I-Sap in normal BALB/c mice (n = 3). (B) Quantified accumulation of Sap in tumor and major organs using the gamma counter after iv injection for 6 h in mice bearing 4T1 breast tumor (n = 3, *p < 0.05, **p < 0.01). (C) CLSM images were taken to show the penetration of fluorescent NG (green) in tumor sections (20 μm thickness). The MB-MDA-231 tumor was incubated with 1.0 mg/mL of NG for 48 h ex vivo. Scale bars: 200 μm. (D) Fluorescence quantification along the arrow in the CLSM images in (C) by ImageJ.

tumor accumulation, which has been reported for other nanovehicles, including silica nanoparticles and polymeric micelles.[45,57,59]

4. CONCLUSIONS

We have demonstrated that small, traceable, endosome-disrupting, and bioresponsive hyaluronic acid NG (HA-NG) mediate CD44-targeted intracellular delivery of therapeutic proteins. With microfluidics and catalyst-free photo-click cross linking, HA-NG can be fabricated with defined and tunable sizes ranging from 80 to 160 nm, strong green fluorescence, and efficient loading of different proteins. Interestingly, HA-NG with a smaller size (80 nm) reveals a clearly better cellular uptake, accelerated endosomal escape, and significantly greater tumor uptake as well as penetration in MDA-MB-231 human breast tumor xenografts in comparison with their 150 nm counterparts. By introducing a pH-sensitive fusogenic peptide, GALA, the endosome escape and antiproliferation effect of Sap-NG in different cancer cells can further be boosted. These small, CD44-targeting, endosome-disrupting, and bioresponsive NG with easy and controlled fabrication hold a great potential for targeted protein therapy.

ASSOCIATED CONTENT

Supporting Information

The Supporting Information is available free of charge on the ACS Publications website at DOI: 10.1021/acsami.9b05827.

Materials, synthetic route, UV spectra, DLS measurement, cytotoxicity of blank NG, and in vivo fluorescence images (PDF)

AUTHOR INFORMATION

Corresponding Authors

*E-mail: cdeng@suda.edu.cn (C.D.).
*E-mail: zyzhong@suda.edu.cn (Z.Z.).

ORCID

Chao Deng: 0000-0001-7697-9874
Zhiyuan Zhong: 0000-0003-4175-4741

Notes

The authors declare no competing financial interest.

ACKNOWLEDGMENTS

This work was supported by the National Natural Science Foundation of China (NSFC 51773145, 51473110, 51633005, and 51603139), the Natural Science Foundation of Jiangsu Province (BK20160307), and a Project Funded by the Priority Academic Program Development of Jiangsu Higher Education Institutions.

REFERENCES

(1) Walsh, G. Biopharmaceutical benchmarks 2018. *Nat. Biotech.* **2018**, *36*, 1136−1145.
(2) Yu, M.; Wu, J.; Shi, J.; Farokhzad, O. C. Nanotechnology for protein delivery: Overview and perspectives. *J. Controlled Release* **2016**, *240*, 24−37.
(3) Liu, X.; Wu, F.; Ji, Y.; Yin, L. Recent advances in anti-cancer protein/peptide delivery. *Bioconjugate Chem.* **2019**, *30*, 305−324.
(4) Lu, Y.; Sun, W.; Gu, Z. Stimuli-responsive nanomaterials for therapeutic protein delivery. *J. Controlled Release* **2014**, *194*, 1−19.
(5) Zhang, P.; He, D.; Klein, P. M.; Liu, X.; Röder, R.; Döblinger, M.; Wagner, E. Enhanced intracellular protein transduction by sequence defined tetra-oleoyl oligoaminoamides targeted for cancer therapy. *Adv. Funct. Mater.* **2015**, *25*, 6627−6636.
(6) Wang, M.; Alberti, K.; Sun, S.; Arellano, C. L.; Xu, Q. Combinatorially designed lipid-like nanoparticles for intracellular delivery of cytotoxic protein for cancer therapy. *Angew. Chem., Int. Ed.* **2014**, *53*, 2893−2898.
(7) Zhang, X.; Malhotra, S.; Molina, M.; Haag, R. Micro- and nanogels with labile crosslinks - from synthesis to biomedical applications. *Chem. Soc. Rev.* **2015**, *44*, 1948−1973.
(8) Li, Y.; Maciel, D.; Rodrigues, J.; Shi, X.; Tomás, H. Biodegradable polymer nanogels for drug/nucleic acid delivery. *Chem. Rev.* **2015**, *115*, 8564−8608.
(9) Li, D.; van Nostrum, C. F.; Mastrobattista, E.; Vermonden, T.; Hennink, W. E. Nanogels for intracellular delivery of biotherapeutics. *J. Controlled Release* **2017**, *259*, 16−28.
(10) Ekkelenkamp, A. E.; Elzes, M. R.; Engbersen, J. F. J.; Paulusse, J. M. J. Responsive crosslinked polymer nanogels for imaging and therapeutics delivery. *J. Mater. Chem. B* **2018**, *6*, 210−235.
(11) Jiang, Y.; Chen, J.; Deng, C.; Suuronen, E. J.; Zhong, Z. Click hydrogels, microgels and nanogels: Emerging platforms for drug delivery and tissue engineering. *Biomaterials* **2014**, *35*, 4969−4985.
(12) Park, H.; Choi, Y.; Jeena, M. T.; Ahn, E.; Choi, Y.; Kang, M.-G.; Lee, C. G.; Kwon, T.-H.; Rhee, H.-W.; Ryu, J.-H.; Kim, B.-S. Reduction-triggered self-cross-linked hyperbranched polyglycerol nanogels for intracellular delivery of drugs and proteins. *Macromol. Biosci.* **2018**, *18*, 1700356.

DOI: 10.1021/acsami.9b05827
ACS Appl. Mater. Interfaces 2019, 11, 22171−22180

(13) Zilkowski, I.; Theodorou, I.; Albrecht, K.; Ducongé, F.; Groll, J. Subtle changes in network composition impact the biodistribution and tumor accumulation of nanogels. *Chem. Commun.* **2018**, *54*, 11777−11780.
(14) Huang, D.; Qian, H.; Qiao, H.; Chen, W.; Feijen, J.; Zhong, Z. Bioresponsive functional nanogels as an emerging platform for cancer therapy. *Expert Opin. Drug Delivery* **2018**, *15*, 703−716.
(15) Su, S.; Wang, Y. Y.; Du, F. S.; Lu, H.; Li, Z. C. Dynamic Covalent Bond-Assisted Programmed and Traceless Protein Release: High Loading Nanogel for Systemic and Cytosolic Delivery. *Adv. Funct. Mater.* **2018**, *28*, 1805287.
(16) Dey, P.; Bergmann, T.; Cuellar-Camacho, J. L.; Ehrmann, S.; Chowdhury, M. S.; Zhang, M.; Dahmani, I.; Haag, R.; Azab, W. Multivalent flexible nanogels exhibit broad-spectrum antiviral activity by blocking virus entry. *ACS Nano* **2018**, *12*, 6429−6442.
(17) Zhu, Q.; Chen, X.; Xu, X.; Zhang, Y.; Zhang, C.; Mo, R. Tumor-specific self-degradable nanogels as potential carriers for systemic delivery of anticancer proteins. *Adv. Funct. Mater.* **2018**, *28*, 1707371.
(18) Min, K.-I.; Kim, D.-H.; Lee, H.-J.; Lin, L.; Kim, D.-P. Direct synthesis of a covalently self-assembled peptide nanogel from a tyrosine-rich peptide monomer and its biomineralized hybrids. *Angew. Chem., Int. Ed.* **2018**, *57*, 5630−5634.
(19) Chen, Y.; Tezcan, O.; Li, D.; Beztsinna, N.; Lou, B.; Etrych, T.; Ulbrich, K.; Metselaar, J. M.; Lammers, T.; Hennink, W. E. Overcoming multidrug resistance using folate receptor-targeted and pH-responsive polymeric nanogels containing covalently entrapped doxorubicin. *Nanoscale* **2017**, *9*, 10404−10419.
(20) De Backer, L.; Braeckmans, K.; Stuart, M. C. A.; Demeester, J.; De Smedt, S. C.; Raemdonck, K. Bio-inspired pulmonary surfactant-modified nanogels: A promising siRNA delivery system. *J. Controlled Release* **2015**, *206*, 177−186.
(21) Sanjay, S. T.; Zhou, W.; Dou, M.; Tavakoli, H.; Ma, L.; Xu, F.; Li, X. Recent advances of controlled drug delivery using microfluidic platforms. *Adv. Drug Delivery Rev.* **2018**, *128*, 3−28.
(22) Ahn, J.; Ko, J.; Lee, S.; Yu, J.; Kim, Y.; Jeon, N. L. Microfluidics in nanoparticle drug delivery; From synthesis to pre-clinical screening. *Adv. Drug Delivery Rev.* **2018**, *128*, 29−53.
(23) Riahi, R.; Tamayol, A.; Shaegh, S. A. M.; Ghaemmaghami, A. M.; Dokmeci, M. R.; Khademhosseini, A. Microfluidics for advanced drug delivery systems. *Curr. Opin. Chem. Eng.* **2015**, *7*, 101−112.
(24) Ma, J.; Lee, S. M.-Y.; Yi, C.; Li, C.-W. Controllable synthesis of functional nanoparticles by microfluidic platforms for biomedical applications - a review. *Lab Chip* **2017**, *17*, 209−226.
(25) Zhao, M.; Liu, Y.; Hsieh, R. S.; Wang, N.; Tai, W.; Joo, K.-I.; Wang, P.; Gu, Z.; Tang, Y. Clickable protein nanocapsules for targeted delivery of recombinant p53 protein. *J. Am. Chem. Soc.* **2014**, *136*, 15319−15325.
(26) Chen, J.; Ouyang, J.; Chen, Q.; Deng, C.; Meng, F.; Zhang, J.; Cheng, R.; Lan, Q.; Zhong, Z. EGFR and CD44 dual-targeted multifunctional hyaluronic acid nanogels boost protein delivery to ovarian and breast cancers in vitro and in vivo. *ACS Appl. Mater. Interfaces* **2017**, *9*, 24140−24147.
(27) Li, S.; Zhang, T.; Xu, W.; Ding, J.; Yin, F.; Xu, J.; Sun, W.; Wang, H.; Sun, M.; Cai, Z.; Hua, Y. Sarcoma-targeting peptide-decorated polypeptide nanogel intracellularly delivers shikonin for upregulated osteosarcoma necroptosis and diminished pulmonary metastasis. *Theranostics* **2018**, *8*, 1361−1375.
(28) Liang, K.; Ng, S.; Lee, F.; Lim, J.; Chung, J. E.; Lee, S. S.; Kurisawa, M. Targeted intracellular protein delivery based on hyaluronic acid-green tea catechin nanogels. *Acta Biomater.* **2016**, *33*, 142−152.
(29) Chen, J.; Zou, Y.; Deng, C.; Meng, F.; Zhang, J.; Zhong, Z. Multifunctional click hyaluronic acid nanogels for targeted protein delivery and effective cancer treatment in vivo. *Chem. Mater.* **2016**, *28*, 8792−8799.
(30) Ding, L.; Jiang, Y.; Zhang, J.; Klok, H.-A.; Zhong, Z. pH-Sensitive coiled-coil peptide-cross-linked hyaluronic acid nanogels: Synthesis and targeted intracellular protein delivery to CD44 positive cancer cells. *Biomacromolecules* **2018**, *19*, 555−562.
(31) Stewart, M. P.; Sharei, A.; Ding, X.; Sahay, G.; Langer, R.; Jensen, K. F. In vitro and ex vivo strategies for intracellular delivery. *Nature* **2016**, *538*, 183−192.
(32) Sudo, K.; Niikura, K.; Iwaki, K.; Kohyama, S.; Fujiwara, K.; Doi, N. Human-derived fusogenic peptides for the intracellular delivery of proteins. *J. Controlled Release* **2017**, *255*, 1−11.
(33) Bolhassani, A.; Jafarzade, B. S.; Mardani, G. In vitro and in vivo delivery of therapeutic proteins using cell penetrating peptides. *Peptides* **2017**, *87*, 50−63.
(34) Shang, L.; Cheng, Y.; Zhao, Y. Emerging droplet microfluidics. *Chem. Rev.* **2017**, *117*, 7964−8040.
(35) Lu, M.; Ozcelik, A.; Grigsby, C. L.; Zhao, Y.; Guo, F.; Leong, K. W.; Huang, T. J. Microfluidic hydrodynamic focusing for synthesis of nanomaterials. *Nano Today* **2016**, *11*, 778−792.
(36) Liang, Y.; Peng, J.; Li, N.; Yu-Wai-Man, C.; Wang, Q.; Xu, Y.; Wang, H.; Tagalakis, A. D.; Du, Z. Smart nanoparticles assembled by endogenous molecules for siRNA delivery and cancer therapy via CD44 and EGFR dual-targeting. *Nanomedicine* **2019**, *15*, 208−217.
(37) Khalil, I. A.; Harashima, H. An efficient PEGylated gene delivery system with improved targeting: Synergism between octaarginine and a fusogenic peptide. *Int. J. Pharm.* **2018**, *538*, 179−187.
(38) Inada, T.; Tamura, A.; Terauchi, M.; Yamaguchi, S.; Yui, N. A silencing-mediated enhancement of osteogenic differentiation by supramolecular ternary siRNA polyplexes comprising biocleavable cationic polyrotaxanes and anionic fusogenic peptides. *Biomater. Sci.* **2018**, *6*, 440−450.
(39) Kim, Y.; Lee Chung, B.; Ma, M.; Mulder, W. J. M.; Fayad, Z. A.; Farokhzad, O. C.; Langer, R. Mass production and size control of lipid-polymer hybrid nanoparticles through controlled microvortices. *Nano Lett.* **2012**, *12*, 3587−3591.
(40) Estupiñán, D.; Barner-Kowollik, C.; Barner, L. Counting the clicks in fluorescent polymer networks. *Angew. Chem., Int. Ed.* **2018**, *57*, 5925−5929.
(41) Chen, J.; Huang, K.; Chen, Q.; Deng, C.; Zhang, J.; Zhong, Z. Tailor-making fluorescent hyaluronic acid microgels via combining microfluidics and photoclick chemistry for sustained and localized delivery of herceptin in tumors. *ACS Appl. Mater. Interfaces* **2018**, *10*, 3929−3937.
(42) Li, S.; Zhang, J.; Deng, C.; Meng, F.; Yu, L.; Zhong, Z. Redox-sensitive and intrinsically fluorescent photoclick hyaluronic acid nanogels for traceable and targeted delivery of cytochrome c to breast tumor in mice. *ACS Appl. Mater. Interfaces* **2016**, *8*, 21155−21162.
(43) Water, J. J.; Kim, Y.; Maltesen, M. J.; Franzyk, H.; Foged, C.; Nielsen, H. M. Hyaluronic Acid-Based Nanogels Produced by Microfluidics-Facilitated Self-Assembly Improves the Safety Profile of the Cationic Host Defense Peptide Novicidin. *Pharm. Res.* **2015**, *32*, 2727−2735.
(44) Bazban-Shotorbani, S.; Dashtimoghadam, E.; Karkhaneh, A.; Hasani-Sadrabadi, M. M.; Jacob, K. I. Microfluidic directed synthesis of alginate nanogels with tunable pore size for efficient protein delivery. *Langmuir* **2016**, *32*, 4996−5003.
(45) Tang, L.; Gabrielson, N. P.; Uckun, F. M.; Fan, T. M.; Cheng, J. Size-dependent tumor penetration and in vivo efficacy of monodisperse drug-silica nanoconjugates. *Mol. Pharm.* **2013**, *10*, 883−892.
(46) Wang, J.; Mao, W.; Lock, L. L.; Tang, J.; Sui, M.; Sun, W.; Cui, H.; Xu, D.; Shen, Y. The role of micelle size in tumor accumulation, penetration, and treatment. *ACS Nano* **2015**, *9*, 7195−7206.
(47) Salatin, S.; Maleki Dizaj, S.; Yari Khosroushahi, A. Effect of the surface modification, size, and shape on cellular uptake of nanoparticles. *Cell Biol. Int.* **2015**, *39*, 881−890.
(48) Hoshyar, N.; Gray, S.; Han, H.; Bao, G. The effect of nanoparticle size on *in vivo* pharmacokinetics and cellular interaction. *Nanomedicine* **2016**, *11*, 673−692.
(49) Santiwarangkool, S.; Akita, H.; Nakatani, T.; Kusumoto, K.; Kimura, H.; Suzuki, M.; Nishimura, M.; Sato, Y.; Harashima, H. PEGylation of the GALA peptide enhances the lung-targeting activity

DOI: 10.1021/acsami.9b05827
ACS Appl. Mater. Interfaces 2019, 11, 22171−22180

of nanocarriers that contain encapsulated siRNA. *J. Pharm. Sci.* **2017**, *106*, 2420−2427.
(50) Yao, P.; Zhang, Y.; Meng, H.; Sun, H.; Zhong, Z. Smart polymersomes dually functionalized with cRGD and fusogenic GALA peptides enable specific and high-efficiency cytosolic delivery of apoptotic proteins. *Biomacromolecules* **2018**, *20*, 184.
(51) Wan, Y.; Moyle, P. M.; Christie, M. P.; Toth, I. Nanosized, peptide-based multicomponent DNA delivery systems: Optimization of endosome escape activity. *Nanomedicine* **2016**, *11*, 907−919.
(52) Bi, C.; Miao, X. Q.; Chow, S. F.; Wu, W. J.; Yan, R.; Liao, Y. H.; Chow, A. H.-L.; Zheng, Y. Particle size effect of curcumin nanosuspensions on cytotoxicity, cellular internalization, in vivo pharmacokinetics and biodistribution. *Nanomedicine* **2017**, *13*, 943−953.
(53) Perrault, S. D.; Walkey, C.; Jennings, T.; Fischer, H. C.; Chan, W. C. W. Mediating tumor targeting efficiency of nanoparticles through design. *Nano Lett.* **2009**, *9*, 1909−1915.
(54) Popović, Z.; Liu, W.; Chauhan, V. P.; Lee, J.; Wong, C.; Greytak, A. B.; Insin, N.; Nocera, D. G.; Fukumura, D.; Jain, R. K.; Bawendi, M. G. A nanoparticle size series for in vivo fluorescence imaging. *Angew. Chem., Int. Ed.* **2010**, *49*, 8649−8652.
(55) Arranja, A. G.; Pathak, V.; Lammers, T.; Shi, Y. Tumor-targeted nanomedicines for cancer theranostics. *Pharmacol. Res.* **2017**, *115*, 87−95.
(56) Duan, X.; Li, Y. Physicochemical characteristics of nanoparticles affect circulation, biodistribution, cellular internalization, and trafficking. *Small* **2013**, *9*, 1521−1532.
(57) Cabral, H.; Matsumoto, Y.; Mizuno, K.; Chen, Q.; Murakami, M.; Kimura, M.; Terada, Y.; Kano, M. R.; Miyazono, K.; Uesaka, M.; Nishiyama, N.; Kataoka, K. Accumulation of sub-100 nm polymeric micelles in poorly permeable tumours depends on size. *Nat. Nanotechnol.* **2011**, *6*, 815−823.
(58) Tang, L.; Yang, X.; Yin, Q.; Cai, K.; Wang, H.; Chaudhury, I.; Yao, C.; Zhou, Q.; Kwon, M.; Hartman, J. A.; Dobrucki, I. T.; Dobrucki, L. W.; Borst, L. B.; Lezmi, S.; Helferich, W. G.; Ferguson, A. L.; Fan, T. M.; Cheng, J. Investigating the optimal size of anticancer nanomedicine. *Proc. Natl. Acad. Sci. U.S.A.* **2014**, *111*, 15344−15349.
(59) Tang, L.; Fan, T. M.; Borst, L. B.; Cheng, J. Synthesis and Biological Response of Size-Specific, Monodisperse Drug-Silica Nanoconjugates. *ACS Nano* **2012**, *6*, 3954−3966.

DOI: 10.1021/acsami.9b05827
ACS Appl. Mater. Interfaces 2019, 11, 22171−22180